Available online at www.sciencedirect.com
ScienceDirect
Ceramics International 37 (2011) 1147–1152
CERAMICS INTERNATIONAL
www.elsevier.com/locate/ceramint

Artificial neural network investigation of hardness and fracture toughness of hydroxylapatite

Zafer Evis [a,*], Erol Arcaklioglu [b]

[a] Middle East Technical University, Department of Engineering Sciences, Ankara 06531, Turkey
[b] Karabuk University, Department of Mechanical Engineering, Karabuk, Turkey

Received 28 June 2010; received in revised form 18 August 2010; accepted 26 October 2010
Available online 15 December 2010

Abstract

Hardness and fracture toughness of hydroxylapatite were investigated by artificial neural network (ANN). Hardness and fracture toughness of hydroxylapatite were predicted by using its sintering temperature, sintering time, relative density, and grain size with ANN. It was found that prediction results of its hardness and fracture toughness closely matched with the experimental results.

Keywords: C. Hardness; Hydroxylapatite; Fracture toughness; Artificial neural network

1. Introduction

Hydroxylapatite (HA, $Ca_{10}(PO_4)_6(OH)_2$) has been widely used in orthopedic applications because of its excellent biocompatibility and its similar chemical composition to the inorganic part of the bone. Due to these properties of HA, the main application areas of HA are composite materials and implant coatings.

Sintering temperature is one of the several parameters influencing the sintering process. It has a strong relationship with mechanical properties of HA. The presence of the phases, densification behaviour, and grain sizes of HA is some of the other properties which affect the mechanical properties of sintered HA [1–4]. Densification of HA is generally succeeded by compaction and sintering. Uniaxial pressing is mostly used to achieve compaction; however, it leads to loss of uniformity of sintered body and generates crack formation throughout the body [5]. The compacted HA powders sintered at temperatures between 900 °C and 1200 °C for 1 h under compaction of 600 MPa showed an increase in its density [6]. Although HA can be fully densified at 1100 °C, its sintering higher than 1150 °C may result in decomposition of HA into (α or β) tri-calcium phosphate (TCP) [7,8]. Grain growth of HA generally occurs during sintering above 1100 °C [9]. Retardation of grain growth of HA was achieved by spark plasma sintering process for short durations [10]. Moreover, dense HA (∼50 nm grain size) was produced by pressure assisted sintering at 900 °C [11].

The mechanical properties of HA, such as hardness and fracture toughness, are considerably affected by sintering conditions. For example, fracture toughness and hardness of HA increased by 40% and over 200% at sintering temperatures ranging from 1000 °C to 1400 °C, respectively [12]. A study on sintering of HA in different environments showed that the Knoop hardness of HA sintered in vacuum was lower than that of HA sintered in air [7]. Furthermore, the lowest hardness value was obtained for HA sintered in humid air [7]. Moreover, the hardness and fracture toughness of HA depend on not only the sintering temperature but also porosity, grain size and purity of HA [3,4,10,13–16]. For example, the decrease in density of HA and increasing the sintering temperature above 1400 °C were due to the grain growth phenomenon and severe decomposition of HA and there is a correlation between hardness and grain size, i.e. the hardness of HA would decrease as a result of grain growth above a critical grain size [4], also decomposition of HA was detrimental to hardness properties of HA, as well as, to fracture toughness [4]. Although some studies stated that the dependence of hardness on grain size, Hoepfner and Case [16] reported that there was no clear grain size dependence on hardness. In fact, the hardness values of HA decreased rapidly as porosity of the material increased [16].

* Corresponding author. Tel.: +90 312 210 4450; fax: +90 312 210 4462.
E-mail address: evis@metu.edu.tr (Z. Evis).

0272-8842/$36.00
doi:10.1016/j.ceramint.2010.10.037

Artificial neural network (ANN) has been successfully applied in various fields of mathematics, engineering, medicine, economics, meteorology, and psychology. This system comprises operators interconnected via one-way signal flow channels. It collects the samples with a distributed coding which forms a trainable non-linear system. It is also self-adaptive to the environment to respond to the different inputs rationally. ANN was applied on various properties of HAs and apatites to estimate lattice constants of the apatites and to provide alternative ways for selection and design of biomaterials [17–20]. Various apatite formulas were derived from the prediction of lattice parameters by using average ionic radii by ANN because the crystal structure of apatite is too complex to determine by only using experimental techniques [17,18]. Moreover, ANN was used to predict the wear behaviours of HA and stainless steel composites [19]. Furthermore, mechanical strength and setting times of HA cements were predicted by using ANN [20].

In this study, hardness and fracture toughness of HA were investigated by ANN for the first time. Effect of sintering temperature, sintering time, relative density, and grain size of HA on its hardness and fracture toughness was simulated by ANN. The learning algorithm called back-propagation was applied for single hidden layer. Scaled Conjugate Gradient (SCG) and Levenberg–Marquardt (LM) were used for the variants of the algorithm.

2. Methods: determination of data and the artificial neural network model

In this study, data received from Refs. [2,15,16,21–26] were used to train and test an artificial neural network. Sintering temperature (T), sintering time (Ti), relative density (D), and grain size (GS) were used as input parameters to determine the hardness and fracture toughness of the HAs. Following characterization methods could be used to determine the density of the samples, grain size of the samples and to determine whether the sintered samples are pure HA or not.

The density of the samples was calculated by dividing the weight by the volume. A scanning electron microscope (SEM) is generally used to examine the grain size of the samples. The grain size was determined by the intercept method [27]. Presence of the phases in the samples was characterized by X-ray diffraction (XRD).

There are two outputs which are hardness and fracture toughness in this study. In this study, Vickers micro (μ)-hardness of HAs were collected from the literature. The hardness value for each sample was calculated by:

$$\mathrm{HV} = 0.001854 * \frac{P}{d^2} \tag{1}$$

where HV, Vickers hardness; P, applied load; d, diagonal indent length.

Fracture toughness (K_{1c}) of the HAs was determined from cracks formed in the Vickers μ-hardness test. In pure HAs, Halfpenny shape crack formation was observed and the Evans and Charles equation was used to determine its fracture toughness [28]:

$$K_{1c} = 0.0824 * \frac{P}{C^{1.5}} \tag{2}$$

where P, applied load (N); C, crack length (m).

ANNs are composed of neurons and used to solve complex functions. A neural network system has three layers, namely, the input layer, the hidden layer and the output layer. The input layer consists of all the input factors, information from the input layer is then processed in the course of one hidden layer, and output vector is computed in the output layer. Generally, the hidden and the output layers have an activation function.

An important stage when accommodating a neural network is the training step, in which an input is introduced to the network together with the desired outputs, the weights and bias values are initially chosen randomly and the weights are adjusted so that the network attempts to produce the desired output. The weights, after the training, contain meaningful information, whereas before the training, they are random and have no meaning. When a satisfactory level of performance is reached, the training stops, and the network use these weights to make the decisions.

Many alternative training processes are available, such as back-propagation. The goal of any training algorithm is to minimize the global error level, such as the mean % error (MAPE), Root-Mean-Squared (RMS), and absolute fraction of variance (R^2) [29,30]. An important characteristic of this function is differentiable throughout its domain. The errors for hidden layers are determined by propagating back the error determined for the output layer.

For ANNs two data sets are needed: one for training the network and the second one for testing it. The usual approach is to prepare a single data set, and differentiate it randomly. The list of data values used in this study are listed in Table 1. There are two networks; one is for hardness and the other one is for fracture toughness. T, Ti, D and GS, which represent processing of the HAs (sintering temperature and time) and characteristics (density and grain size depended on processing parameters), were used as input layer while hardness and fracture toughness were used as output layer, respectively.

In this study, the learning algorithm called back-propagation was applied for single hidden layer. SCG and LM were used for the variants of the algorithm. Normalization values for both inputs and outputs were used between the values of 0 and 1. Neurons in input layer had no transfer function. Logistic sigmoid (logsig) transfer function was also used:

$$F(z) = \frac{1}{1 + \exp(-z)} \tag{3}$$

where z is the weighted sum of the input.

ANN was trained and tested by MATLAB software. To identify the output precisely for the training stage, increased number of neurons (3–5) in hidden layer was tried. Firstly, the network was trained successfully, and then the test data was used to test the network. In the training stage, to identify the output with a success, number of neurons was increased from 3 to 5 using the trial and error method in the hidden layer. Among

Table 1
Data used in the ANN studies of HAs hardness and fracture toughness [2,15,16,21–26].

Sintering temp. (°C)	Sintering time (h)	Relative density (%)	Grain size	Hardness (GPa)	Fracture toughness (MPa$\sqrt{m}$)
850	0.083	90.3	2.82		1.15
900	2	83.0	0.12		0.95
900	0.083	96.9	2.91		1.18
900	2	83.3	0.83	3.32	
950	0.083	99.6	3.91		1.25
1000	0.083	99.4	4.86		1.20
1000	2	97.1	0.34		1.21
1000	2	97.0	0.33		1.22
1000	0.5	90.8	0.13		1.23
1000	2	96.1	1.25	4.45	
1000	2	99	0.88	5.91	
1050	2	98.2	0.50		1.16
1050	2	98.1	0.46		1.16
1050	0.5	95.2	0.14		1.44
1050	2	98.3	0.53	7.21	
1050	7	99.4	1.72	5.01	
1050	2	98.4	5.13	5.76	
1050	2	98.1	0.46	7.21	
1100	2	71.8	0.57		0.70
1100	3	96.8	1.20		0.79
1100	2	98.6	0.63		1.14
1100	2	98.7	0.69		1.15
1100	0.083	99.1	5.18		1.22
1100	12	99.3	1.94	4.8	
1100	2	97.2	6.29	4.26	
1150	2	83.3	0.83		0.95
1150	2	99.0	0.88		1.05
1150	0.5	96.6	0.34		1.14
1150	2	98.6	0.63	7	
1150	2	97	5.7	4.82	
1150	2	83	0.12	2.8	
1150	2	98.6	7.13	5.75	
1150	2	99	0.88	6.65	
1150	2	90.3	0.714	4.273	
1200	2	96.1	1.25		0.69

them, the network with 4 neurons and 3 neurons including a single hidden layer provided the best hardness and fracture toughness results, respectively. Therefore, the results presented in this study are based on this configuration. After training the network successfully, test data was used to test the network. Using the results extracted by the network, a comparison was made using statistical methods.

Errors formed at the learning and testing stages were described as RMS and R^2, maximum and mean error percentage values, respectively, which are shown in the following equations:

$$\mathrm{RMS} = \left(\left(\frac{1}{p} \right) \sum_j \left| t_j - o_j \right|^2 \right)^{1/2} \quad (4)$$

$$R^2 = 1 - \left(\frac{\sum_j (t_j - o_j)^2}{\sum_j (o_j)^2} \right) \quad (5)$$

$$\text{Mean \% error} = \frac{1}{p} \sum_j \left(\frac{t_j - o_j}{t_j} * 100 \right) \quad (6)$$

where t is the target value, o is the output value, and p is the pattern [31].

3. Results and discussion

XRD results of dried and sintered HA powders are presented in Fig. 1. Dried HA displayed wide and low intensity peaks, which is indicative of small constituent particle sizes. In contrast, the XRD peaks for the HA sintered at 900 °C, 1100 °C, and 1300 °C for 1 h were sharp and narrow, showing that the HA grain size increased after sintering. They had similar crystalline peaks to the pure HA. This showed that HA synthesized by precipitation method is very resistant to high sintering temperatures. Sintering time of 1 h is short enough for HA not to decompose. If HA is sintered above 1100 °C with a sintering time longer than 1 h, it starts to decompose to TCP as seen in reaction (7).

$$Ca_{10}(PO_4)_6(OH)_2 \rightarrow 3Ca_3(PO_4)_2 + CaO + H_2O \quad (7)$$

In Fig. 2, SEM micrographs of dense and 11% porous HA are presented. As seen from these two images, the grain sizes were much smaller than 1 μm.

In the training, we used an increased number of neurons (from 3 to 5) in hidden layer to define the output accurately for SCG and LM algorithms. The best algorithms are LM with 4 neurons for hardness and LM with 3 neurons for fracture

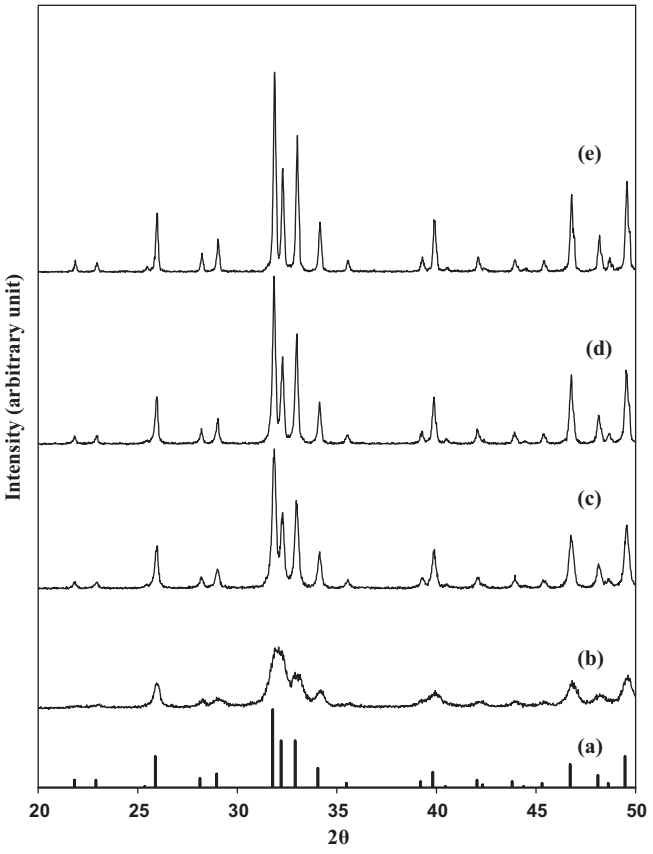

Fig. 1. X-ray diffraction spectra of (a) HA standards (JCPDS # 9-432); (b) HA dried at 200 °C; (c) HA sintered at 900 °C for 1 h; (d) HA sintered at 1100 °C for 1 h; and (e) HA sintered at 1300 °C for 1 h.

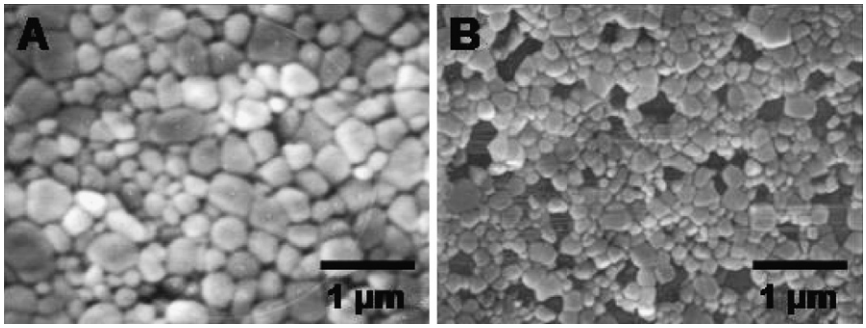

Fig. 2. SEM micrographs of (A) dense HA and (B) 11% porous HA.

toughness, respectively. After this point, all explanations, tables and figures were given for the two algorithms.

Figs. 3 and 4 compare the actual and the ANN predicted hardness values for training and testing using LM with 4 hidden neurons which produced much better results than other algorithms with various hidden layers mentioned before. As shown in these figures a high correlation exists between the actual and the predicted data indicating a successful learning by the proposed ANN model.

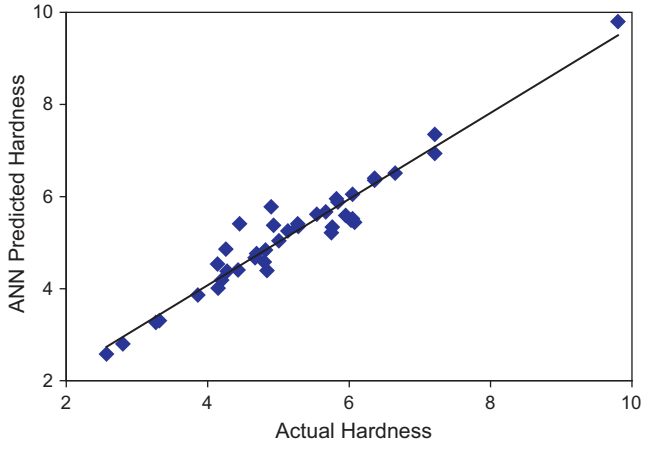

Fig. 3. Comparison of actual and predicted results for hardness for the training data (LM4).

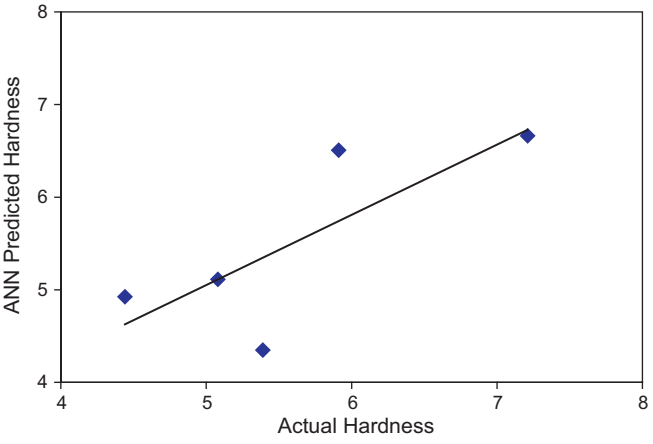

Fig. 4. Comparison of actual and predicted results for hardness for the test data (LM4).

Figs. 5 and 6 compare the actual and the ANN predicted fracture toughness values for training and testing using LM with 3 hidden neurons. As shown in these figures a high correlation exists between the actual and the predicted data indicating a successful learning by the proposed ANN model.

In Table 2, the statistical values of the outputs for this algorithm are shown for both training and testing data. Error values of the outputs are also given in this table. In Table 2, the RMS, R^2 and MAPE values for both training and testing stages are illustrated very well within an acceptable range.

The formulations of the fracture toughness and hardness outputs are given in Eqs. (8) and (9), respectively. Using these formulas the fracture toughness and hardness value of an HA may be calculated within the error range given in Table 2. The advantage of using these formulations is that, they only consist of four mathematical operations.

$$\text{Fracture toughness} = \frac{1}{1 + e^{-(0.8352F1 + 120.9005F2 - 117.9145F3 - 0.4619)}} \tag{8}$$

$$\text{Hardness} = \frac{1}{1 + e^{-(2.9553F1 - 2.4229F2 - 5.2532F3 - 0.5324F4 + 2.8445)}} \tag{9}$$

The equations in Tables 3 and 4 depend on sintering temperature, sintering time, density (or porosity), and grain

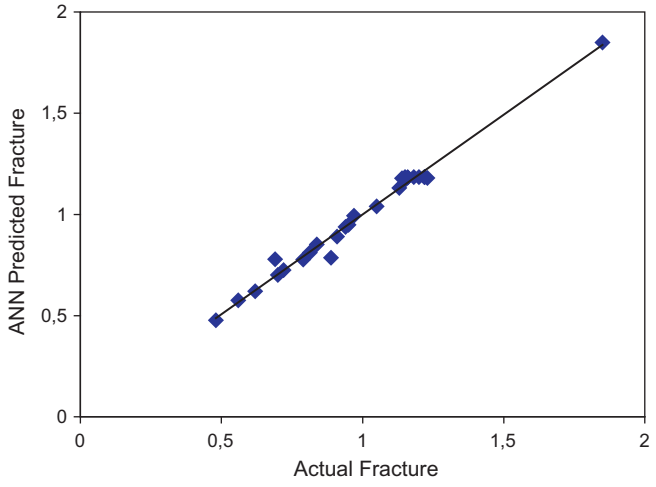

Fig. 5. Comparison of actual and predicted results for fracture toughness for the training data (LM3).

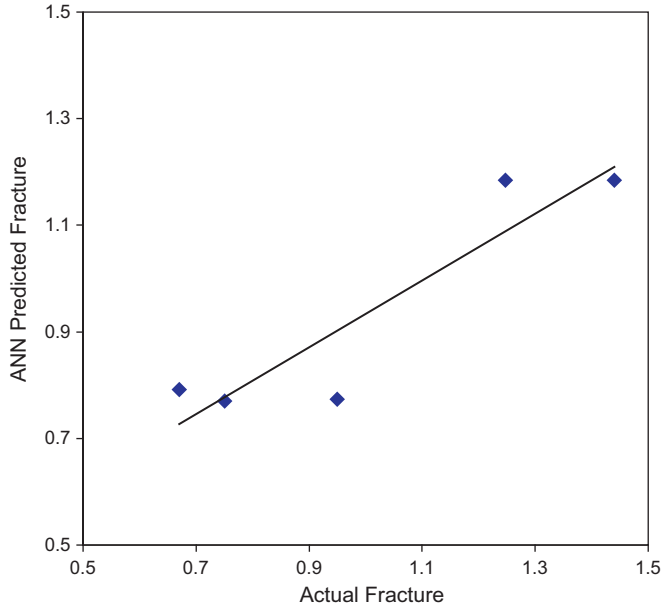

Fig. 6. Comparison of actual and predicted results for fracture toughness for the test data (LM3).

size, which are the inputs of the network. Coefficients in Eqs. (8) and (9) are the weights, which lie between the hidden and output layers. When using the equations in Tables 3 and 4, T and D values were normalized by dividing them with 1700, and 20, respectively, to obtain the emissions and performance values in Eqs. (8) and (9), fracture toughness and hardness values were multiplied by 2 and 12, respectively.

The basic indicators (X) in input layer such as Ti and GS were normalized according to Eq. (10). The X_{min} and X_{max} values for basic indicators are given in Table 5.

$$X = 0.8 \times \left[\frac{X_{actual} - X_{min}}{X_{max} - X_{min}}\right] + 0.1 \quad (10)$$

Obviously, the advantage of using the above formulations is that they only consist of basic mathematical operations. The network was employed to make further predictions for different T, Ti, D, and GS.

Out of four inputs (sintering temperature, sintering time, density, and grain size of HA), it was found that the predicted outputs (hardness and fracture toughness of HA) showed a very

Table 2
Statistical values of predictions.

Outputs	Algorithm and hidden number	RMS training	R^2 training	Mean % error training	RMS test	R^2 test	Mean % error test
Fracture toughness	LM 3	0.016459	0.998974	2.2545	0.076086	0.97911	12.450
Hardness	LM 4	0.027464	0.996202	4.0837	0.052361	0.987776	9.709

Table 3
The weights between the input and hidden layer for fracture toughness.

i	$E_i = C_1*T + C_2*Ti + C_3*D + C_4*\mathrm{GS} + C_5$				
	C_1	C_2	C_3	C_4	C_5
1	−119.8742	−42.3467	199.6448	45.0252	−73.5761
2	61.0407	4.3962	−62.9536	0.6705	−2.0380
3	60.1879	5.5483	−64.9102	3.7551	−0.9633

Table 4
The weights between the input and hidden layer for hardness.

i	$E_i = C_1*T + C_2*Ti + C_3*D + C_4*\mathrm{GS} + C_5$				
	C_1	C_2	C_3	C_4	C_5
1	−78.9447	5.2538	−76.2570	18.7195	110.9555
2	−229.1155	60.2938	−803.9789	−254.6757	821.1240
3	−0.2987	1.5519	−9.8568	0.5896	8.2775
4	−412.2968	−242.3685	222.9680	−190.2741	122.8381

Table 5
Values for normalization.

	X_{min}	X_{max}
Time (Ti) for fracture toughness	0	6
Time (Ti) for hardness	0	25
Grain size (GS) for fracture toughness	0	20
Grain size (GS) for hardness	0	28

good agreement with the experimental findings. Although, we used four different inputs to find the outputs, we can also add other parameters which can probably affect the mechanical properties of HA. For example, presence of second phases, amount of dopings and different synthesis methods could also be factors in determining the mechanical properties of HA.

4. Conclusion

This study provided important results for researchers working on HA to improve its mechanical strength. Material characterization studies revealed that altered chemistry, maintenance of HA crystallinity, amount of porosity in HA, and smaller grain sizes may be responsible for hardness and fracture toughness. From the ANN predictions found in this study, we can predict the hardness and fracture toughness of HA if we know its sintering temperature, sintering time, grain size and relative density without performing the mechanical tests.

References

[1] I. Mobasherpour, M.S. Heshajin, A. Kazemzadeh, M. Zakeri, Synthesis of nanocrystalline hydroxyapatite by using precipitation method, J. Alloys Compd. 430 (2007) 330–333.
[2] N. Thangamani, K. Chinnakali, F.D. Gnanam, The effect of powder processing on densification, microstructure and mechanical properties of hydroxyapatite, Ceram. Int. 28 (2002) 355–362.
[3] S. Ramesh, C.Y. Tan, I. Sopyan, M. Hamdi, W.D. Teng, Consolidation of nanocrystalline hydroxyapatite powder, Sci. Technol. Adv. Mater. 8 (2007) 124–130.
[4] G. Muralithran, S. Ramesh, The effects of sintering temperature on the properties of hydroxyapatite, Ceram. Int. 26 (2000) 222–230.
[5] G. Muralithran, S. Ramesh, Internal report No. 09-01-01-0014-01, SIRIM Berhad, 1997.
[6] D.K. Pattanayak, R. Dash, R.C. Prasad, B.T. Rao, T.R.R. Mohan, Synthesis and sintered properties evaluation of calcium phosphate ceramics, Mater. Sci. Eng. C 27 (2007) 684–690.
[7] P.E. Wang, T.K. Chaki, Sintering behaviour and mechanical properties of hydroxyapatite and dicalcium phosphate, J. Mater. Sci. Mater. Med. 4 (1993) 150–158.
[8] M. Jarcho, C.H. Bolen, M.B. Thomas, J. Babock, J.F. Kay, R.H. Doremus, Hydroxylapatite synthesis and characterization in dense polycrystalline form, J. Mater. Sci. 11 (1976) 2027–2035.
[9] Z. Evis, Al3+ doped nano-hydroxyapatites and their sintering characteristics, J. Ceram. Soc. Jpn. 114 (2006) 1001–1004.
[10] Y.W. Gu, N.H. Loh, K.A. Khor, S.B. Tor, P. Cheang, Spark plasma sintering of hydroxyapatite powders, Biomaterials 23 (2002) 37–43.
[11] E.S. Ahn, N.J. Gleason, A. Nakahira, J.Y. Ying, Nanostructure processing of hydroxyapatite-based bioceramics, Nano Lett. 1 (2001) 149–153.
[12] P. Van Landuyt, F. Li, J.P. Keustermans, J.M. Streydio, F. Delannay, E. Munting, The influence of high sintering temperatures on the mechanical properties of hydroxylapatite, J. Mater. Sci. Mater. Med. 6 (1995) 8–13.
[13] S. Ramesh, C.Y. Tan, S.B. Bhaduri, W.D. Teng, Rapid densification of nanocrystalline hydroxyapatite for biomedical applications, Ceram. Int. 33 (2007) 1363–1367.
[14] J. Zhang, H. Tanaka, F. Ye, D. Jiang, M. Iwasa, Colloidal processing and sintering of hydroxyapatite, Mater. Chem. Phys. 101 (2007) 69–76.
[15] K.C.B. Yeong, J. Wang, S.C. Ng, Fabricating densified hydroxyapatite ceramics from a precipitated precursor, Mater. Lett. 38 (1999) 208–213.
[16] T.P. Hoepfner, E.D. Case, The influence of the microstructure on the hardness of sintered hydroxyapatite, Ceram. Int. 29 (2003) 699–706.
[17] P. Wu, Y.Z. Zeng, C.M. Wang, Prediction of apatite lattice constants from their constituent elemental radii and artificial intelligence methods, Biomaterials 25 (2004) 1123–1130.
[18] U. Kockan, Z. Evis, Prediction of hexagonal lattice parameters of various apatites by artificial neural networks, J. Appl. Crystallogr. 43 (2010) 769–779.
[19] M. Younesi, M.E. Bahrololoom, M. Ahmadzadeh, Prediciton of wear behavious of nickel free stainless steel-hydroxyapatite bio-composites using artificial neural network, Comp. Mater. Sci. 47 (2010) 645–654.
[20] H. Baseri, S.M. Rabiee, F. Moztarzadeh, M. Solati-Hashjin, Mechanical strength and setting times estimation of hydroxyapatite cement by using neural network, Mater. Des. 31 (2010) 2585–2591.
[21] C.K. Wang, C.P. Ju, J.H. Chern Lin, Effect of doped bioactive glass on structure and properties of sintered hydroxyapatite, Mater. Chem. Phys. 53 (1998) 138–149.
[22] S. Ramesh, C.Y. Tan, C.L. Peralta, W.D. Teng, The effect of manganese oxide on the sinterability of hydroxyapatite, Sci. Technol. Adv. Mater. 8 (2007) 257–263.
[23] J.A. Delgado, L. Morejon, S. Martinez, M.P. Ginebra, N. Carlsson, E. Fernandez, J.A. Planell, M.T. Clavaguera-Mora, J. Rodriguez-Viejo, Zirconia-toughened hydroxyapatite ceramic obtained by wet sintering, J. Mater. Sci. Mater. Med. 10 (1999) 715–719.
[24] C.Y. Chiu, H.C. Hsu, W.H. Tuan, Effect of zirconia addition on the microstructural evolution of porous hydroxyapatite, Ceram. Int. 33 (2007) 715–718.
[25] B. Chen, T. Zhang, J. Zhang, Q. Lin, D. Jiang, Microstructure and mechanical properties of hydroxyapatite obtained by gel-casting process, Ceram. Int. 34 (2008) 359–364.
[26] D.C. Tancred, B.A.O. McCormack, A.J. Carr, A quantitative study of the sintering and mechanical properties of hydroxyapatite phosphate glass composites, Biomaterials 19 (1998) 1735–1743.
[27] J.E. Hilliard, Estimating Grain Size by the Intercept Method, Metal Prog. Data Sheet (1964) 99.
[28] C.B. Ponton, R.D. Rawlings, Vickers indentation fracture toughness test Part I. Review of literature and formulation of standardized indentation toughness equation, Mater. Sci. Technol. 5 (1989) 865–872.
[29] A. Sozen, E. Arcaklioglu, M. Ozkaymak, Turkey's net energy consumption, Appl. Energy 81 (2005) 209–221.
[30] E.N. Dizdar, Uygulamalı Olasılık ve Istatistik, ABP Yayınevi&Matbaacilik, 2004 (in Turkish).
[31] M. Pala, E. Ozbay, A. Oztas, M.I. Yuce, Appraisal of long-term effects of fly ash and silica fume on compressive strength of concrete by neural networks, Constr. Build. Mater. 21 (2007) 384–394.